

N65-88650

Article for AIAA Magazine - Astronautics and Aerospace Engineering, June Issue

30P

AERODYNAMICS OF THE PARAWING

By William C. Sleeman, Jr., and Joseph L. Johnson, Jr. (Spangley)

The National Aeronautics and Space Administration has been conducting research investigations to provide information on the aerodynamic characteristics of parawings. A wide range of applications of the parawing concept is currently being considered and consequently a fairly broad spectrum of configurations has been investigated. Use of the tension structure concept for flexible wings, which was pioneered by F. M. Rogallo of the Langley Research Center, has offered a possible means of recovery and landing of spacecraft since this type of wing can be packaged and deployed in a manner similar to recovery parachutes, and in addition provides attractive glide and landing flare capabilities. Other uses of the parawing concept that are presently being considered are cargo dropping, cargo towing, rocket booster recovery, powered reconnaissance drone, and manned utility vehicle. A considerable amount of low-speed aerodynamic information has been obtained in research support for specific applications and from basic parameteric general-research investigations. A list of published information from these research investigations is given in references 1 to 12.

Some aerodynamic data on parawings have been selected for presentation herein to summarize some of the most recent aerodynamic information on parawings obtained at the Langley Research Center. The state-of-the-art with regard to lift-drag ratio is summarized and emphasis is given to considerations of fundamental factors affecting the performance, stability, and control of parawing operations. In addition to the experimental data, the results of related

FACILITY FORM 802

N65-88650  
(ACCESSION NUMBER)

30  
(PAGES)

TMX-57480  
(NASA CR OR TMX OR AD NUMBER)

(THRU)

(CODE)

(CATEGORY)

2-5859

analytical studies and some comparisons with conventional wing theory are also presented.

Lift and drag characteristics.- Some typical lift and drag characteristics of a large-scale inflated-tube parawing configuration are presented in figure 1(a) as a function of angle of attack of the wing keel. The lift curve is quite non-linear between angles of attack of about  $-5^{\circ}$  to  $15^{\circ}$ . This characteristic is associated with unloading of the canopy, which is referred to as luffing and will be discussed later. For angles above  $15^{\circ}$ , the lift increased up to the maximum test angle of  $56^{\circ}$ . There was no evidence of wing stall and the highest lift coefficient attained was 1.3. The drag data showed a high value of minimum drag as would be expected from a configuration having large diameter leading edges (diameters approximately 12-percent keel length at the apex, tapering to 4.8-percent keel at the tip). The maximum lift-drag (L/D) ratio obtained for this configuration was approximately 3.5.

Attainment of higher L/D ratios than those shown for the configuration of figure 1(a) is highly desirable; it is appropriate therefore to consider some of the basic geometric parameters affecting L/D. Inasmuch as the leading-edge size was a contributing factor to the relatively low values of L/D obtained on the model of figure 1(a), effects of leading-edge size on L/D are summarized in figure 1(b). These test results were obtained on an inflated-tube configuration which had untapered leading edges and keel, and had a spreader bar to maintain the sweep angle of  $55^{\circ}$ . The results presented in figure 1(b) show a progressive increase in L/D as the size of the leading edge and keel was reduced. The highest value of L/D obtained was about 4.4 for the wing with a leading-edge diameter of 1.5-percent keel length. The dotted curve shown in figure 1(b) indicates an ideal variation of L/D which represents an upper

boundary for wings of the given sweep and aspect ratio. An estimated skin-friction drag coefficient for the canopy of 0.013, and the assumption of full leading-edge suction was used in determination of the drag coefficients. It is evident from comparison of experiment with the ideal curve that even with the smallest leading edges tested, the parawings were far short of the lift-drag ratio potential for this wing planform. One phase of NASA research has been accordingly directed toward attaining wing configurations that realize more fully the lift-drag ratio potential of the wings.

Figure 2 has been prepared to illustrate some important geometric characteristics of parawings that have a significant influence on lift-drag ratio. On the left-hand side of figure 2 is illustrated the conical-shaped canopy obtained on conventional parawings. The shape of these canopies is defined by the flat pattern sweep of the canopy fabric  $\Lambda_0$  and the flight sweep  $\Lambda$ . When the leading-edge sweep is increased from  $\Lambda_0$  to  $\Lambda$  (see sketch A), the canopy develops two lobes and the surface of the canopy lies on two cones which intersect at the apex as shown in figure 2. Below the sketch in figure 2 is illustrated the variation of geometric twist across one of the canopy lobes, and it is seen that the washout increases with spanwise distance from the keel. For canopies having deep lobes ( $\Lambda = 10^\circ$  to  $15^\circ$  greater than  $\Lambda_0$ ) the washout at the tip may be as high as  $50^\circ$ . The type of span loading obtained with conical-shaped canopies is illustrated at the bottom of figure 2 for a wing-lift coefficient of 0.4. The high washout in the wing causes the wing to carry negative lift near the tip. This type of span loading causes high induced drag and is a major factor responsible for the relatively low values of  $(L/D)_{\max}$  shown in figure 1(b).

One approach to improving the lift-drag ratios of parawings would be to reduce the twist by having very shallow lobes ( $\Lambda_0 \approx \Lambda$ ) to provide an almost flat wing. This approach would however require a more rigid structure and depart from the parawing tension structure concept. Another approach is to form the wing about cylinders, parallel to the keel as shown in the right-hand portion of figure 2. This type of wing has a helical-shaped leading edge and has a variation of dihedral across the span. The streamwise airfoil sections, however, lie on the surface of the cylinder, are parallel to the keel, and have no twist or camber. The more nearly elliptical span loading for this type of wing should result in less induced drag and higher maximum lift-drag ratios than for the wings having conical-shaped canopies.

Lift-drag ratios for parawings having both conical and cylindrical canopy shapes are summarized in figure 3(a). All of these wings had rigid, streamlined leading edges and the sweep angle of  $50^\circ$  was maintained by a spreader bar. Test results are presented for parawings having aspect ratios of 2.57 (equal length leading edges and keel) and 5.45 and these results show the gain in  $(L/D)_{\max}$  expected from an increase in wing-aspect ratio. Results for these wings also indicated that appreciable increases in  $(L/D)_{\max}$  were obtained on both the low- and high-aspect-ratio wings by use of the cylindrical canopy shape. A maximum value of lift-drag ratio of 13.6 was obtained for the aspect-ratio-5.45 wing with the cylindrical canopy shape. Both of the cylindrical wings, however, had lower values of  $L/D$  at high lift than the corresponding conical wings. This characteristic which apparently results from tip stalling of the untwisted wings indicates that the washout of the conical wings was favorable at high lift.

Although use of the cylindrical wings resulted in considerable improvement in maximum lift-to-drag ratio relative to the very highly twisted and cambered

conical wings, some moderate washout would be expected to improve the span-load distribution and performance of these highly tapered wings. Results are presented in figure 3(b) to show effects on  $(L/D)_{\max}$  of adding a small amount of washout to an aspect-ratio-5.45 cylindrical wing. The addition of washout was accomplished by adding some fullness to the trailing edge of the untwisted cylindrical wing, and the amount of this fullness is defined here by the flat pattern sweep. The flat pattern sweep of  $48.2^\circ$  gave the basic zero twist condition at  $\Lambda = 50^\circ$  and reduction of the flat pattern sweep allowed the trailing edge to rise above its basic position to provide a small amount of washout. Figure 3(b) shows that addition of some washout increased the maximum lift-drag ratio to a value slightly above 16.0 for a flat pattern sweep of  $46^\circ$ . The decrease of  $(L/D)_{\max}$  with further addition of washout indicates that there is an optimum amount of washout for this wing, with regard to  $(L/D)_{\max}$ .

It should be pointed out that any particular wing shown in figure 3 should not be considered an optimum wing because many factors other than  $L/D$  have to be considered in the selection of a wing. Structural-weight trade-offs, for example, and the intended application for the wing will have an important bearing on the selection of a wing. Other factors such as stability and control characteristics are also important in the selection of a wing, and these considerations will be discussed later in this paper.

Procedures for estimating the longitudinal aerodynamic characteristics of conventional airplane wings have been refined to the point where fairly reliable predictions can be made of such characteristics as lift-curve slope, span loading, angle of attack for zero lift, pitching moment at zero lift, and wing-alone pitching-moment slope. It is desirable to determine to what extent these established estimation procedures for conventional wings can be used for flexible

parawings. At present only a few checks have been made for parawings, and in general the estimates of the aforementioned wing characteristics have been found to be in fairly good agreement with experiment. One such comparison is presented in figure 4 to show experimental and estimated lift characteristics for cylindrical and conical wings of aspect ratio 5.45.

The comparison of experimental lift characteristics presented in the left-hand portion of figure 4 shows a large difference in keel angle of attack for zero lift between the conical and cylindrical wings. Although there are some differences between the experimental and estimated angle for zero lift, the theory gave a good estimate of the change in zero-lift angle in going from the conical to the cylindrical wing. The difference between test data and theory shown for a given wing probably occurred because the actual flexible wing did not have the true conical or cylindrical shapes that were assumed for the estimates.

Another point of interest shown in figure 4 is the difference in operational lift-coefficient range for the two canopy shapes. The cylindrical wing could be tested near zero lift ( $\alpha = 0^\circ$ ) and there was no canopy luffing throughout the test angle-of-attack range. The conical wing, on the other hand, was limited in the minimum lift coefficient that could be obtained without appreciable canopy deformation and flapping, and this minimum lift coefficient can be considered to define the lower boundary of the normal operational range of the wing with regard to canopy behavior. Experience with a range of wing sweep and conical canopy shapes has indicated in general that the minimum operational lift coefficient is approximately 0.4. (It will be shown later that the minimum operational lift coefficient for cylindrical-canopy wings may be determined by pitching moment rather than lift characteristics.)

The estimated and experimental lift-curve slopes presented in the left-hand plot of figure 4 are in good agreement for both canopy shapes. In order to allow comparisons for a large range of wing planforms, a summary of lift-curve slopes is given in the right-hand portion of figure 4. The form of presentation was selected to allow the use of any sweep or aspect ratio and to indicate approximately the value of section lift slope  $a_0$  to be used in the theory. The comparisons shown have been limited to test data obtained at a fairly high dynamic pressure and for which check runs have substantiated to be fairly accurate data. The present comparison of experimental and theoretical lift-curve slopes indicates that a section lift slope  $a_0$  of approximately 0.09 would be expected to yield a good estimate of wing-lift slope when used in the theory of reference 13.

Longitudinal stability characteristics.- Pitching-moment characteristics are summarized for several parawing configurations in figure 5. The upper left-hand portion shows results for the large-scale inflated-tube configuration previously discussed in figure 1. Pitching moments of the wing alone are presented about a moment reference on the keel and indicate that the wing has a negative pitching moment at zero angle of attack and does not trim. This characteristic is fairly common to low-aspect-ratio parawings with conical canopies, so that in most typical parawing applications, the center of gravity has to be located an appreciable distance below the keel in order to have both trim and stability at positive lift. Pitching moments about the configuration center of gravity located  $0.50l_k$  below the wing showed that the configuration trimmed at a keel angle of attack of  $26^\circ$  and was highly stable from about  $15^\circ$  to  $56^\circ$ . In the low angle-of-attack range the model was highly unstable and was operating in the range of canopy luffing mentioned in connection with figures 1 and 4.

The results in the top right hand of figure 5 show pitching-moment characteristics of the family of wings for which the  $L/D$  summary was presented in figure 3. The moment reference for all of these wings was located at the same position below the keel ( $z/b = 0.3$ ). The longitudinal position of the assumed center of gravity was located to provide trim at a lift coefficient of 0.5, which was an average  $C_L$  for  $(L/D)_{\max}$  for the four wings. These results show that all of the wings could be trimmed and, with the exception of the aspect-ratio-5.45 cylindrical wing, had positive stability over most of the operational lift range. The high-aspect-ratio cylindrical wing showed the well-known loss of static longitudinal stability at moderate lift encountered on many swept wings. Static longitudinal stability could be provided over the lift-coefficient range in this case by the use of a much lower center-of-gravity position but such a change would not eliminate the undesirable nonlinearity of the pitching-moment curve. It should be noted that the addition of a small amount of washout which provided an increase in  $(L/D)_{\max}$  for this wing (fig. 3) also was beneficial in delaying and reducing the severity of the unstable break in the pitching moments of the cylindrical wing. The fairly large amount of washout in the high-aspect-ratio conical wing alleviated the tip stall and no loss of stability was indicated up to a lift coefficient of 1.0. The high level of stability shown for this wing could be reduced, if desired, by raising the center of gravity toward the keel.

The pitching-moment data for the family of conical and cylindrical wings were not measured at negative angles of attack, but all of these wings show a tendency toward static instability at low lift coefficients generally similar to that previously discussed for the large-scale, low-aspect-ratio conical wing. For the cylindrical wings, this tendency is somewhat surprising in view of the difference in lift characteristics for the conical and cylindrical wings, at low

angles of attack mentioned earlier in connection with figure 4. It appears that the low-lift operational boundary for the cylindrical-canopy wings may therefore be determined by the variation in the pitching-moment characteristics rather than lift characteristics.

Although the low-lift range may be considered outside of the normal operational range for parawings, there are some conditions that could cause a parawing configuration to enter this lift range inadvertently. In the case of the low-aspect-ratio conical wing, which has seen the most use to date, these characteristics at low lift have been found under some conditions in model flight tests to result in an end-over-end tumbling motion.

Some static force test data related to the tumbling problem are presented in the lower plot of figure 5. Pitching-moment characteristics are presented in this plot over a  $360^\circ$  angle-of-attack range for a low-aspect-ratio conical parawing with low center of gravity together with similar data for a conventional delta-wing configuration with the center of gravity in the plane of the wing. The data show that near  $0^\circ$  (and  $360^\circ$ ) angle of attack both configurations are stable and trimmed. In the case of the conventional wing, a disturbance which pitches the wing away from its trim point is opposed by large restoring moments which are symmetrical at positive or negative angles of attack. In the case of the parawing, however, there is a region of static longitudinal instability at low negative angles of attack and large differences in the magnitude of the positive and negative pitching moments over the angle-of-attack range. It is this combination of static instability and asymmetry in the pitching moments which appears to be significant in establishing a steady tumbling motion. For example, a parawing configuration which pitches downward through its trim point to low negative angles of attack will encounter the region of static longitudinal

instability and will therefore tend to pitch downward to even higher negative angles of attack. If the pitching motion is strong enough to overcome both the damping in pitch and the positive restoring moments in the  $300^\circ$  to  $180^\circ$  angle-of-attack range, the pitching motion will continue with energy being fed into the system by the large negative pitching moments in the  $180^\circ$  to  $0^\circ$  angle-of-attack range. It is thus possible for a steady nose-down tumbling motion to be established for a configuration of this type. It should be pointed out, however, that predictions of a tumbling motion cannot be made based on static data alone. There are other factors, such as damping in pitch, mass and inertia characteristics, and the variation in airspeed or dynamic pressure which must be considered in determining stable and unstable boundaries in a dynamic stability problem of this type.

Lateral stability characteristics.- In a typical paraglider vehicle, the fact that the center of gravity lies an appreciable distance below the wing may significantly affect the lateral stability characteristics. For such a vehicle, the stability derivatives involving rolling moment or rolling velocity will reflect the influence of the wing side force and sideslip characteristics to a considerable extent, and, in addition, the axis of least inertia may well be oriented nearly perpendicular to the flight path rather than nearly along the flight path as in more conventional aircraft. While these considerations are of significance with regard to both static and dynamic stability characteristics, only some implications of the static stability derivatives will be discussed in this paper.

The static lateral stability parameters  $C_{n\beta}$  and  $C_{l\beta}$  about the stability axes for the large-scale inflated-tube model of figures 1 and 5, and for the small-scale conical and cylindrical models are presented in figure 6. On the

left-hand side of this figure the data show that the large-scale model was statically directionally stable (positive  $C_{n\beta}$ ) and had large positive values of effective dihedral ( $-C_{l\beta}$ ). The values of these derivatives which increased with increasing lift coefficient, are generally representative for parawing configurations of this type. Presented on the right-hand side of figure 6 is a plot of  $C_{n\beta}$  against  $-C_{l\beta}$  to show the effect of canopy shape and aspect ratio on the static lateral stability parameters of the family of parawings previously discussed. For a plot of this type, combinations of  $C_{n\beta}$  and  $-C_{l\beta}$  which fall in the midportion of the first quadrant are generally desirable from the standpoint of dynamic lateral stability. For example, the low-aspect-ratio conical wing, which has combinations of  $C_{n\beta}$  and  $-C_{l\beta}$  as indicated in figure 6, has been found to have generally satisfactory dynamic lateral stability characteristics. In some cases, however, poor Dutch roll damping has been observed for this parawing configuration when large destabilizing bodies such as boosters were suspended beneath the parawing. In such cases the static directional stability of the combination was probably reduced to very low positive values.

On the basis of the flight test experience to date with the low-aspect-ratio conical wing it would appear that the aspect-ratio-5.45 conical wing, which had slightly higher values of  $C_{n\beta}$  for a given value of  $-C_{l\beta}$ , should generally have satisfactory dynamic lateral stability characteristics. For the cylindrical wings, however, the low values of directional stability in combination with relatively high values of positive dihedral effect could lead to poor or unstable Dutch roll damping. In addition, the low positive values of  $C_{n\beta}$  at moderate lift coefficients and the static instability and negative dihedral effect indicated for the low-aspect-ratio cylindrical wing at  $C_L = 1.0$  (a trend which also occurs for the high-aspect-ratio cylindrical wing at a slightly higher lift

coefficient) point out the possibility of directional stability problems with these wings. On the basis of these results, it appears that some means for providing increased static directional stability for the cylindrical wings will be required in order to insure satisfactory dynamic lateral stability characteristics. Some configuration modifications that have been found effective on conical wings in this respect are the use of auxiliary fins or panels, and lowering the leading edges with respect to the keel.

Longitudinal control characteristics.- Longitudinal control for most para-wing applications currently being considered is accomplished by shifting the center of gravity relative to the wing. Some basic information pertaining to longitudinal control through the center-of-gravity shift control system is illustrated in figure 7. The plot at the left of this figure shows the pitching-moment curves resulting when the center of gravity is shifted forward as illustrated in the sketch from position B to A or rearward from position B to C. When the center of gravity is shifted forward to trim at a lower lift coefficient (point A), an increase in stability is also obtained as indicated by the increased slope of the curve. Conversely, there is a reduction in stability when the para-wing is trimmed to a higher lift coefficient (point C).

For cable-supported payloads, center-of-gravity movement is achieved by changing the lengths of the cables. On other applications where the wing and payload are connected by a rigid truss, center-of-gravity shift is accomplished by relative movement of the payload with respect to the wing about a fixed pivot. For both types of applications the wing pitch characteristics about the pivot (virtual pivot for the cable configuration) are important and the sign of the pitching moment at zero lift  $C_{m_0}$  determines whether the control-force gradients are stable or unstable.

The effects of  $C_{m_0}$  on control forces for the fixed-pivot application are illustrated in figure 7(b) which shows pitching-moment data referred to the wing pivot. Three assumed pitching-moment curves are presented - curve 1 has a positive value of  $C_{m_0}$ , while curves 2 and 3 have a common negative value of  $C_{m_0}$ . For curves 1 and 2 the wing pivot is located at the same point on the wing keel and therefore the curves have the same slope. Curve 3 represents the manner of change in curve 2 when the wing pivot is moved rearward so that zero  $C_{m_{pivot}}$  is obtained at the same value of  $C_L$  as for curve 1. The stick-force characteristics for the three conditions shown indicate that a positive value of  $C_{m_0}$  provides a stable stick-force variation with speed (that is, a pull force is required for trim at the lower speeds and a push force at the higher speeds) whereas an unstable variation is obtained when  $C_{m_0}$  is negative. The sign of  $C_{m_0}$  therefore can be taken in a direct indication of the type of stick-force gradient to be expected for a given wing. A small positive value of  $C_{m_0}$  is usually considered desirable from considerations of handling-qualities and control-force requirements.

Both wing planform and twist distribution have an important influence on the wing pitching moment at zero lift. Some results summarizing these effects for several wing configurations are presented in figure 8. The effects of aspect ratio for  $50^\circ$  swept conical wings having a flat pattern sweep of  $\Lambda_0 = 45^\circ$  are shown in the upper left-hand plot. These results indicate that conical wings having aspect ratios below about 5.0 have negative values of  $C_{m_0}$ ; above  $A = 5$  positive values of  $C_{m_0}$  increase with increasing aspect ratio. The explanation of the variation of  $C_{m_0}$  with aspect ratio shown lies in the relative effects of camber (which contributes  $-C_{m_0}$ ) and twist (which produces a  $+C_{m_0}$ ). At low aspect ratio the camber effect predominates inasmuch as the twist contribution

is a function of the quarter-chord sweep, and this sweep is relatively low at low aspect ratio. The twist contribution arises from a couple produced by an upload near the apex and a download near the wing tips. As the aspect ratio increases, the contribution from this couple increases in proportion to the quarter-chord sweep and becomes larger than the camber contribution at aspect ratios above about 5.0. The experimental results appear to be in fairly good agreement with the theoretical variation of  $C_{m_0}$  with aspect ratio for conical wings. Theory for the cylindrical canopies, of course, would indicate zero  $C_{m_0}$  because these wings were designed to have zero twist and camber. Experimental results, on the other hand, indicate that negative values of  $C_{m_0}$  occur at low aspect ratio and become more negative with increasing aspect ratio. This variation indicates the possibility that under actual test conditions, the cylindrical canopies deformed at the trailing edge in a manner to provide washin at the tips.

Inasmuch as  $C_{m_0}$  is determined by the relative effects of twist and camber, it would be expected that flat pattern sweep, or amount of canopy fullness would have an important effect on  $C_{m_0}$ . The effects of flat pattern sweep for the high-aspect-ratio conical wing are summarized in the upper right-hand portion of figure 8. These results show that even for the high-aspect-ratio wing, negative values of  $C_{m_0}$  may be encountered if the canopy is too full (low flat pattern sweep) and that the value of  $C_{m_0}$  can be increased somewhat by using a tighter canopy ( $\Lambda_0 = 47.5^\circ$ ) than the basic  $\Lambda_0 = 45^\circ$  canopy. Further increases in flat pattern sweep would be expected to remove the favorable twist effect as well as the camber effect.

Some typical stick-force variations are shown at the bottom of figure 8 for the family of wings previously discussed. These results indicate, as would be expected, that the high-aspect-ratio conical wing provided a stable stick-force

gradient, while the other three wings had unstable stick-force gradients. In flight tests of the NASA parawing research vehicle, which employs a low-aspect-ratio conical-canopy wing, an objectionable unstable stick-force gradient was experienced over a large portion of the speed range. In the case of the Gemini parawing recovery system, which also employs the low-aspect-ratio conical wing, an irreversible power boost system is to be used which will mask any unstable stick-force gradient encountered with this system.

Lateral control characteristics.- Some fundamental parameters involved in the lateral center-of-gravity shift or wing-bank control system are illustrated in the sketch and formulas at the upper left of figure 9. The formula for net rolling moment is based on the assumption that when the wing is banked, the lift vector is tilted with the wing and has a lateral component which produces a rolling moment about the center of gravity through the arm  $z/b$ . Since for trim conditions the lateral component of the lift acts behind the center of gravity, it also produces an adverse yawing moment through the arm  $x/b$ . When the sideslip angle resulting from this adverse yawing moment is taken into account, it can be shown that the favorable rolling moment produced by the lift vector is reduced through the effective dihedral parameter  $C_{l\beta}$ . The factor within the brackets

$$\left[ 1 - \frac{-C_{l\beta}}{C_{n\beta} \frac{L}{D}} \right]$$

is designated as the rolling-effectiveness parameter and conveniently expresses the percentage of rolling effectiveness that is actually available for a configuration employing the wing-bank or center-of-gravity shift control system. For configurations having high ratios of  $-C_{l\beta}/C_{n\beta}$  and low values of  $L/D$ , the

rolling effectiveness becomes small and therefore the net rolling moment in such cases is reduced. It should be pointed out that the estimates of rolling effectiveness obtained from the above formula are only approximations since the formula was derived on the basis of static considerations alone. There are other factors such as moments of inertia, inclination of the principal axis of inertia, and dynamic stability derivatives which must also be taken into consideration in the final analysis of the control effectiveness under dynamic conditions.

Presented in the lower left plot of figure 9 are values of rolling-effectiveness factor plotted against net rolling-moment coefficient for the conical and cylindrical parawings of aspect ratio 2.7 and 5.45. The results of this plot show that the low-aspect-ratio conical wing has positive values of the rolling-effectiveness factor from about 0.5 to 0.7. This factor is increased for the aspect-ratio-5.45 conical wing and therefore the net rolling moment produced by wing bank is increased in this case. For the cylindrical wings, it is significant to note that the rolling-effectiveness factor is negative and that the rolling moments produced by wing bank are therefore negative or adverse - that is, banking the wing to the right would produce rolling moments to the left. Analysis indicates that despite the increased values of  $L/D$  for the cylindrical wings an adverse rolling effectiveness in these cases results from the low values of  $C_{n\beta}$  and relatively large values of  $-C_{l\beta}$  inherent in this type of parawing. (See fig. 6.) It appears necessary, therefore, that in order for the wing-bank control system to become effective in these cases, the ratio of  $-C_{l\beta}/C_{n\beta}$  must be reduced considerably through increased  $C_{n\beta}$  or perhaps through the combination of increased  $C_{n\beta}$  and reduced  $-C_{l\beta}$ .

In the plot on the right of figure 9, the roll-control forces experienced with the wing-bank control are compared with those for a wing-tip control which

may be considered equivalent to an aileron control on a conventional wing. Two values of  $z/b$  are shown for the wing-bank control, the value of 0.50 corresponding to that used on the Gemini parawing recovery system and the value of 0.135 corresponding to that used on one research configuration. From this plot it is seen that for a given rolling moment, the control forces with a wing-bank control system will be considerably higher than those with an aileron-like wing-tip control.

[www.australian-hang-gliding-history.com](http://www.australian-hang-gliding-history.com)

SYMBOLS

The coefficients are presented with respect to the stability axis system and the reference area used in reduction of the data was taken as the canopy flat pattern area. Coefficients and symbols used are defined as follows:

A	aspect ratio of projected wing planform, $\frac{b^2}{\text{Projected area}}$
b	projected span of wing, ft
$l_k$	length of the wing keel, ft
y	spanwise distance from keel center line, ft
$C_D$	drag coefficient, $\frac{\text{Drag}}{qS}$
$C_L$	lift coefficient, $\frac{\text{Lift}}{qS}$
$C_m$	pitching-moment coefficient, $\frac{\text{Pitching moment}}{qSl_k}$
$C_{m_0}$	pitching-moment coefficient at zero lift (see fig. 7(b))
$C_n$	yawing-moment coefficient, $\frac{\text{Yawing moment}}{qSb}$
$C_l$	rolling-moment coefficient, $\frac{\text{Rolling moment}}{qSb}$
$C_{n\beta}$	static directional stability parameter, per deg
$C_{l\beta}$	effective dihedral parameter, per deg
q	free-stream dynamic pressure, lb/sq ft
S	area of wing canopy flat pattern, sq ft
V	airspeed, knots
z	distance from center of gravity to wing keel, measured normal to keel unless otherwise indicated, ft
$\alpha$	angle of attack of wing keel, deg

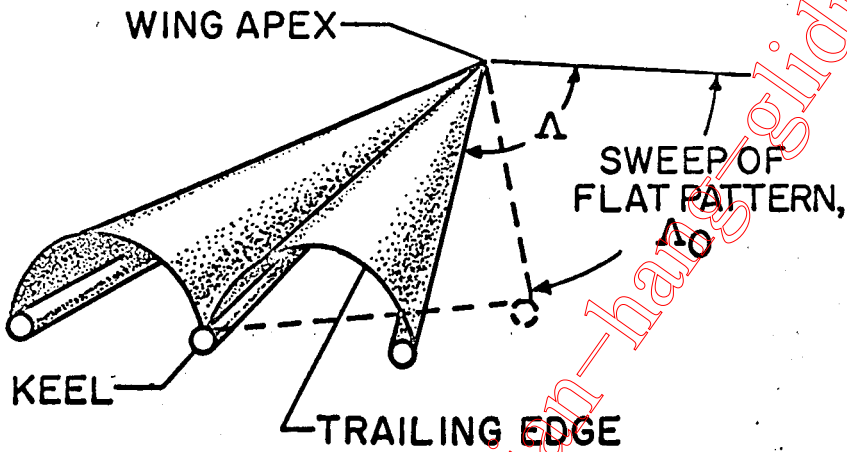
angle of sideslip, deg

sweep of wing leading edge, deg

sweep of leading edge of the canopy flat pattern, deg

sweep of the wing half-chord line, deg

SKETCH A

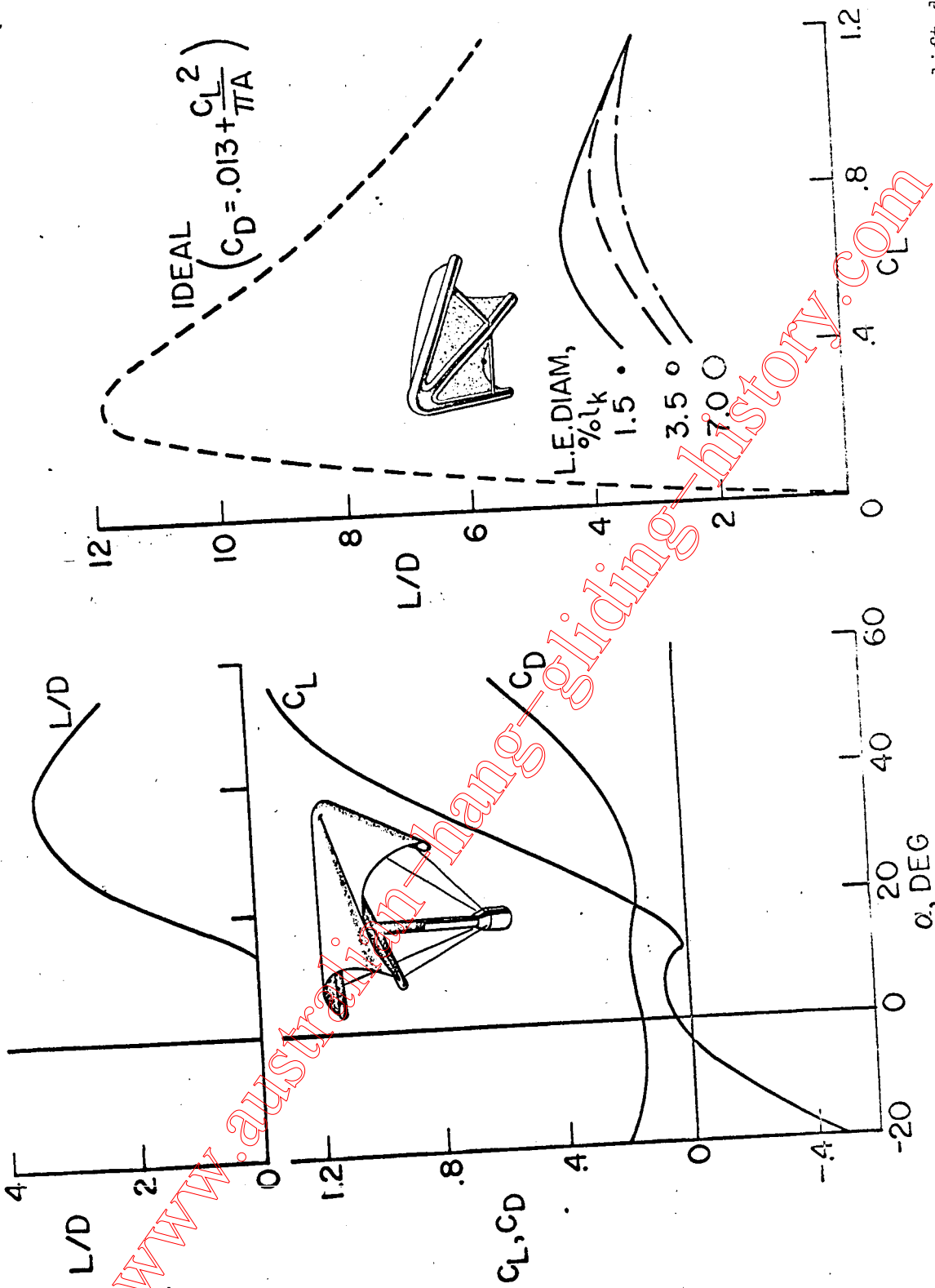


REFERENCES

1. Rogallo, Francis M., Lowry, John G., Croom, Delwin R., and Taylor, Robert T.: Preliminary Investigation of a Paraglider. NASA TN D-443, 1960.
2. Taylor, Robert T.: Wind-Tunnel Investigation of Paraglider Models at Supersonic Speeds. NASA TN D-985, 1961.
3. Penland, Jim A.: A Study of the Aerodynamic Characteristics of a Fixed Geometry Paraglider Configuration and Three Canopies With Simulated Variable Canopy Inflation at a Mach Number of 6.6. NASA TN D-1022, 1961.
4. Naeseth, Rodger L.: An Exploratory Study of a Parawing as a High-Lift Device for Aircraft. NASA TN D-629, 1960.
5. Hewes, Donald E.: Free-Flight Investigation of Radio-Controlled Models With Parawings. NASA TN D-927, 1961.
6. Hatch, Howard G., Jr., and McGowan, William A.: An Analytical Investigation of the Loads, Temperatures, and Ranges Obtained During the Recovery of Rocket Boosters by Means of a Parawing. NASA TN D-1003, 1961.
7. Fournier, Paul G., and Bell, B. Ann: Low Subsonic Pressure Distributions on Three Rigid Wings Simulating Paragliders With Varied Canopy Curvature and Leading-Edge Sweep. NASA TN D-983, 1961.
8. Fournier, Paul G., and Bell, B. Ann: Transonic Pressure Distributions on Three Rigid Wings Simulating Paragliders With Varied Canopy Curvature and Leading-Edge Sweep. NASA TN D-1009, 1961.
9. Fournier, Paul G.: Pressure Distributions on Three Rigid Wings Simulating Parawings With Varied Canopy Curvature and Leading-Edge Sweep at Mach Numbers From 2.29 to 4.65. NASA TN D-1618, 1963.

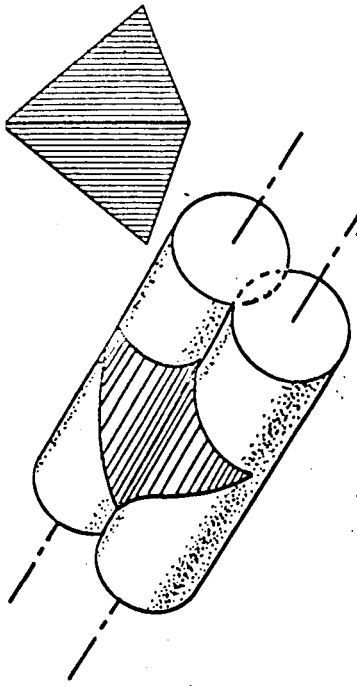
- . Polhamus, Edward C., and Naeseth, Rodger L.: Experimental and Theoretical Studies of the Effects of Camber and Twist on the Aerodynamic Characteristics of Parawings Having Nominal Aspect Ratios of 3 and 6. NASA TN D-972, 1963.
- . Johnson, Joseph L., Jr.: Low-Speed Wind-Tunnel Investigation to Determine the Flight Characteristics of a Model of a Parawing Utility Vehicle. NASA TN D-1255, 1962.
- . Layton, Garrison P., Jr., and Thompson, Milton O.: Preliminary Flight Evaluation of Two Unpowered Manned Paragliders. NASA TN D-1826, 1963.
- . Lowry, John G., and Polhamus, Edward C.: A Method for Predicting Lift Increments Due to Flap Deflection at Low Angles of Attack in Incompressible Flow. NACA TN 3911, 1957.

www.australian-hang-gliding-history.com

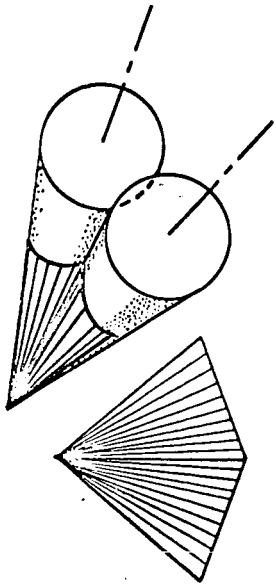
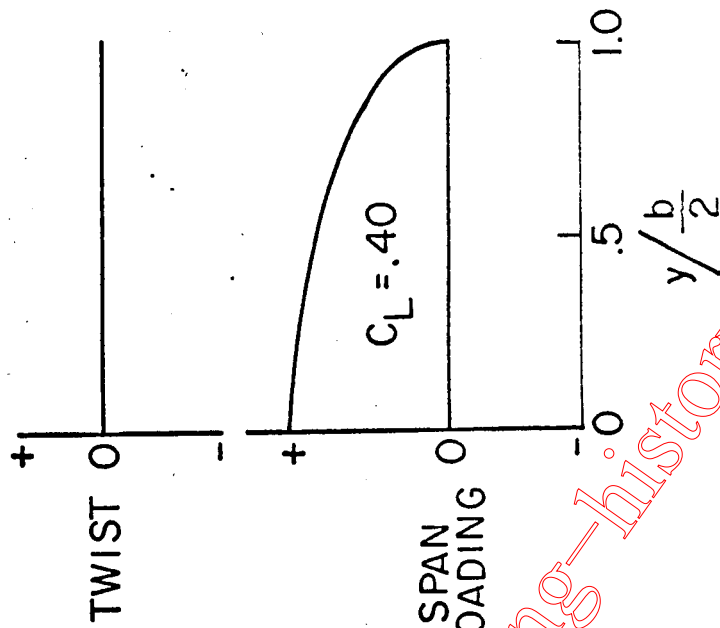


(a) Large-scale tapered-tube model,  $\Lambda = 55^\circ$ . (b) Effect of leading-edge diameter on lift-drag ratio,  $\Lambda = 55^\circ$ .

Figure 1.- Lift and drag characteristics of inflated-tube parawing configurations.



CYLINDRICAL SHAPED CANOPIES



CONICAL SHAPED CANOPIES

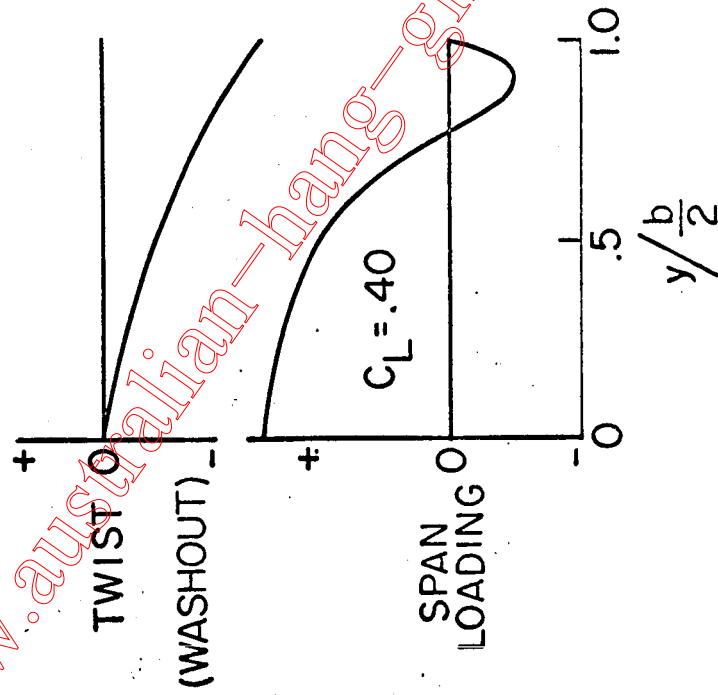
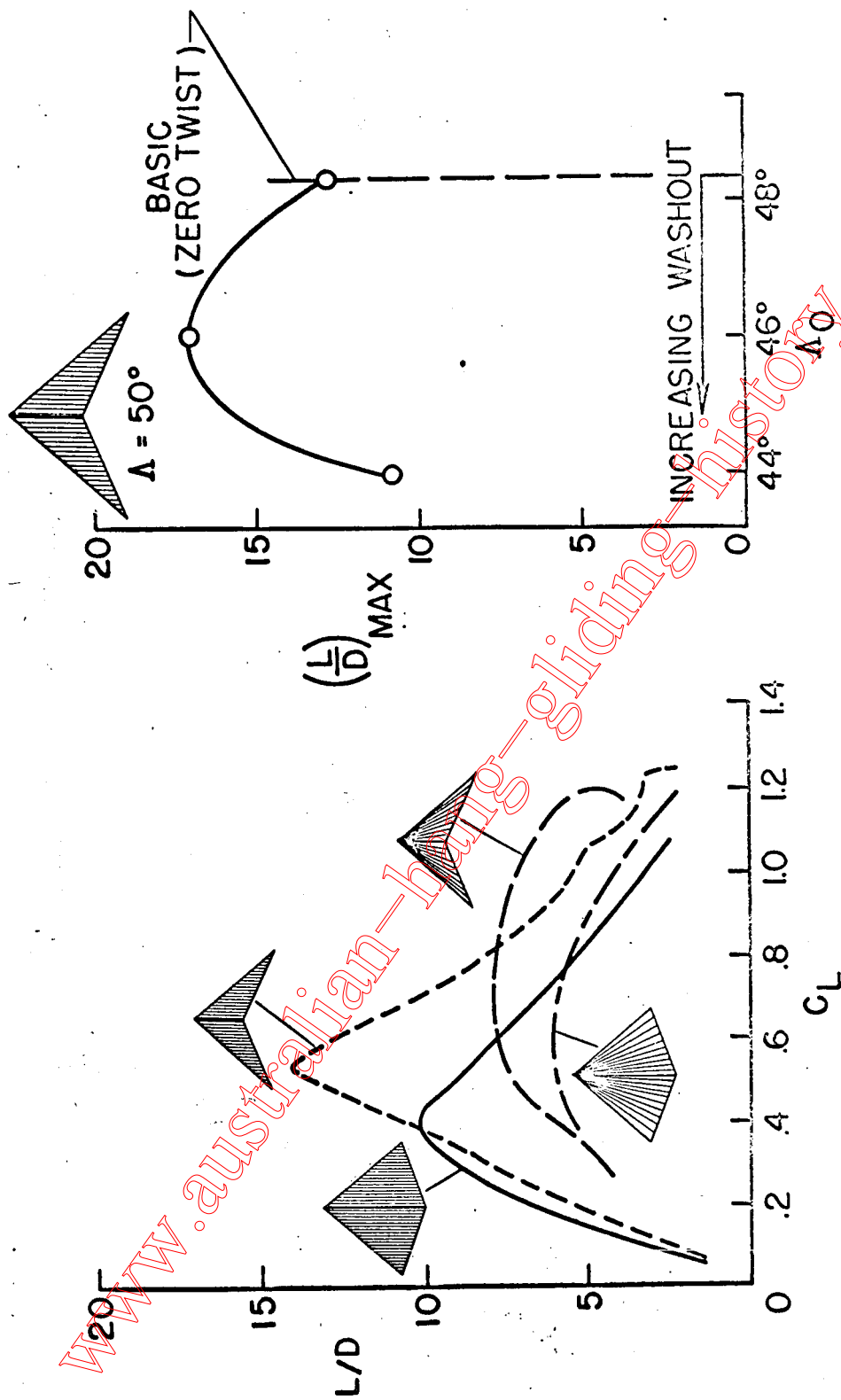


Figure 2.- Geometric twist and span loading for conical and cylindrical-shaped canopies.



(a) Effect of planform and canopy shape.

(b) Effect of adding washout to a basic cylindrical parawing.

Figure 3.- Lift-drag ratios for 50° swept parawings.

— EXPERIMENT  
 — THEORY

○ EXPERIMENT  
 — THEORY

$A=5.45; \Lambda=50^\circ$

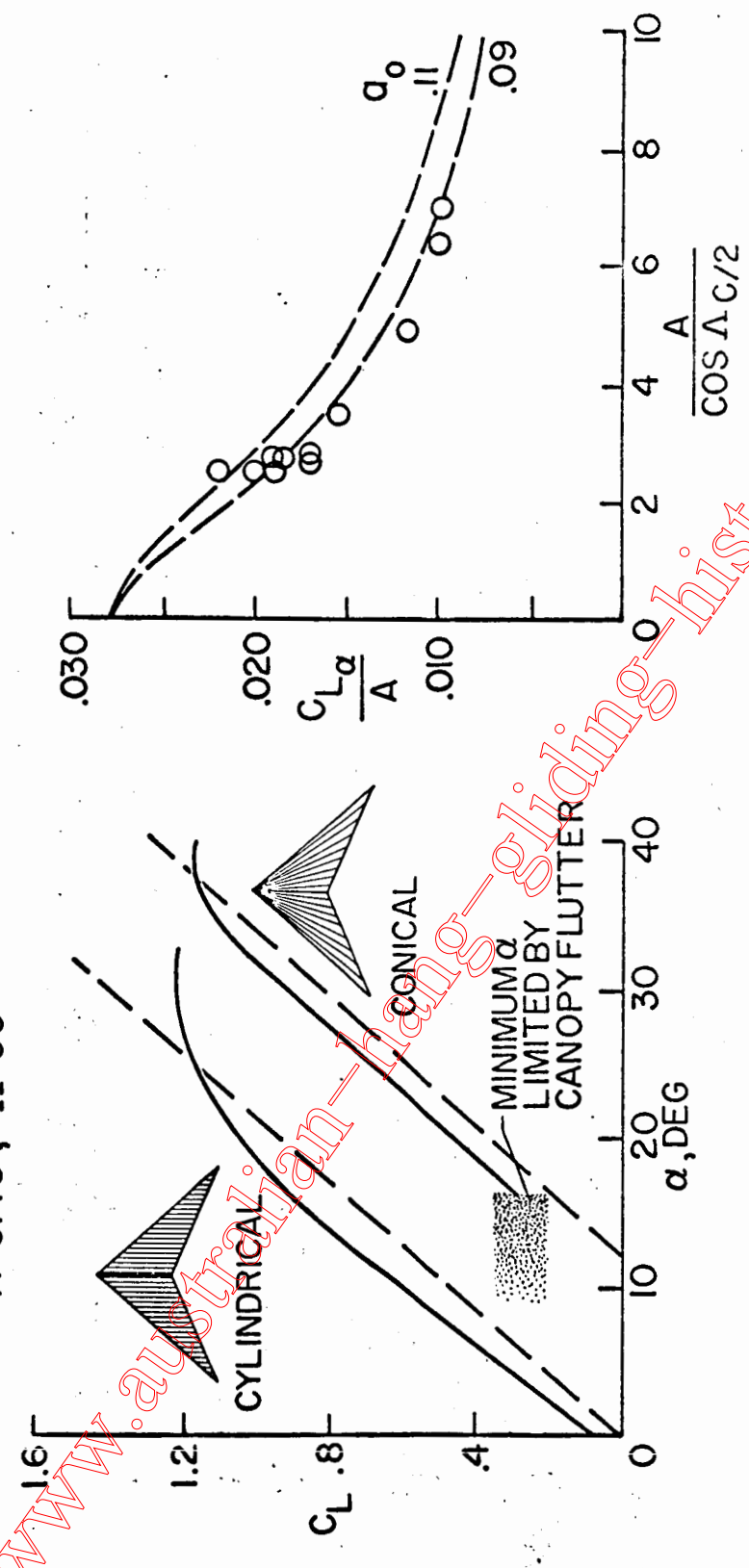
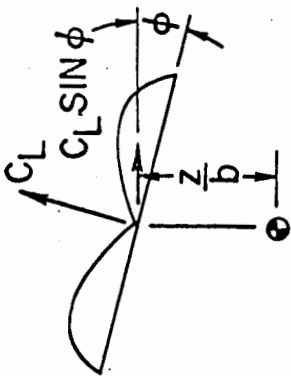
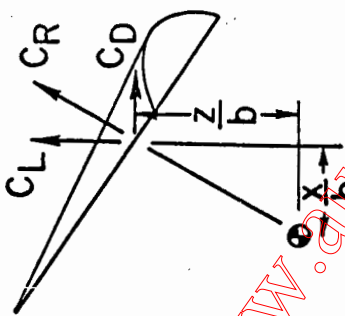
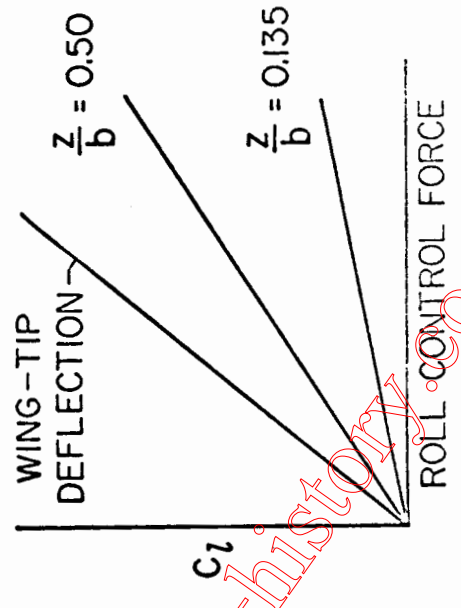
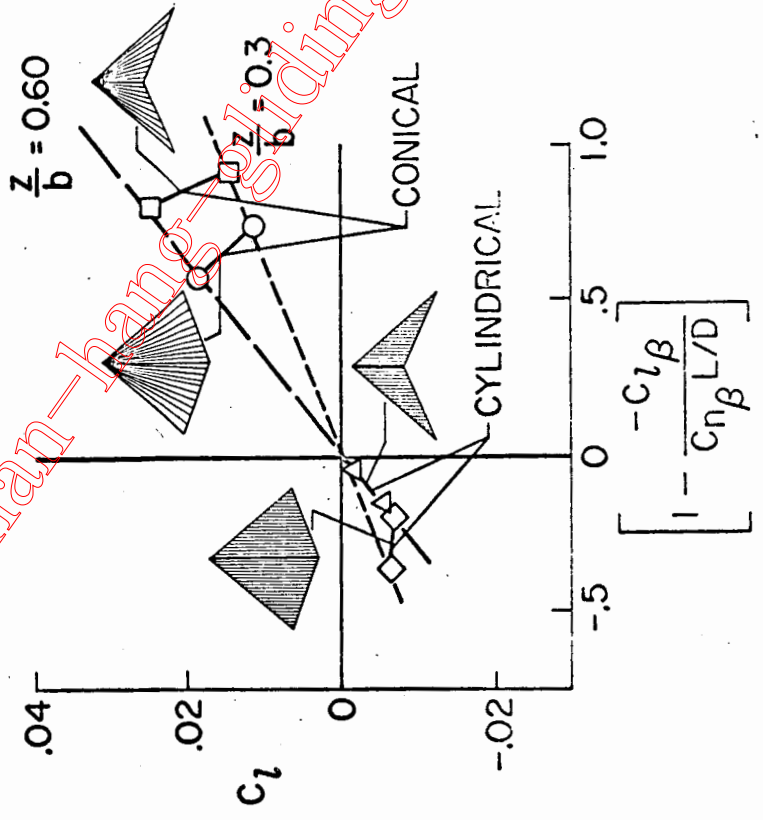


Figure 4.- Comparison of experimental and theoretical lift characteristics of parawings having conical- and cylindrical-shaped canopies.



$$C_n = C_L \sin \phi \frac{x}{b}$$

$$C_l = C_L \sin \phi \frac{z}{b} \left[ 1 - \frac{-C_{l\beta}}{C_{n\beta} L/D} \right]$$



www.Australian-hang-gliding-history.com

Figure 9.- Lateral control characteristics of parawings.

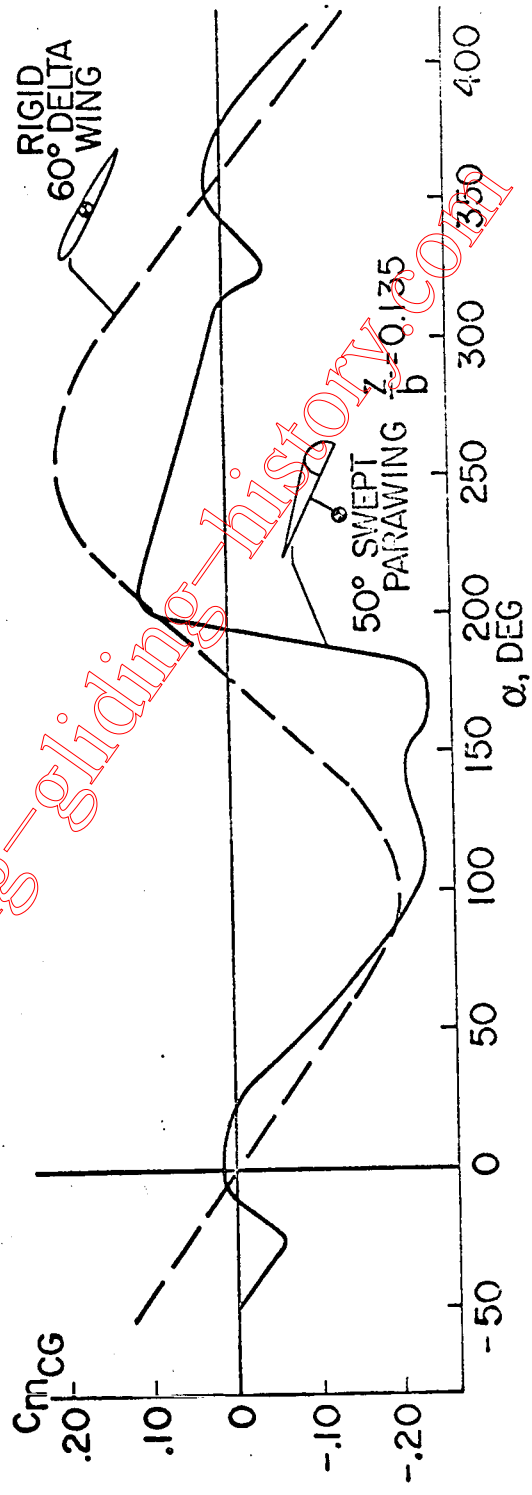
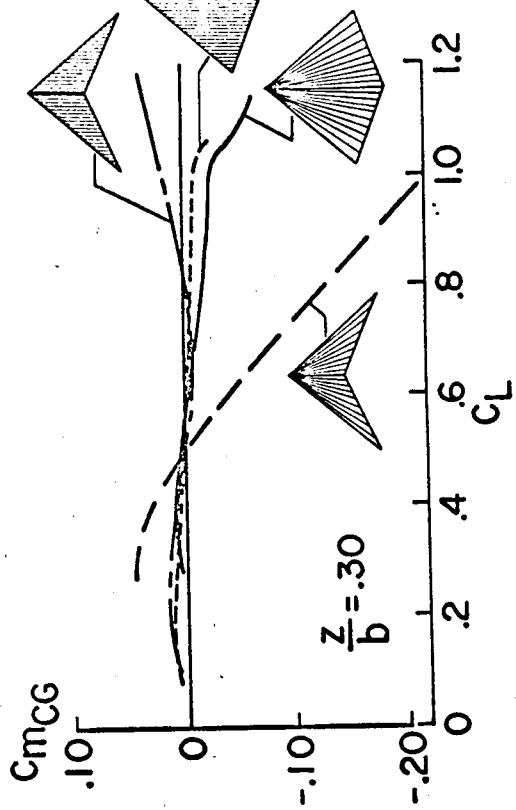
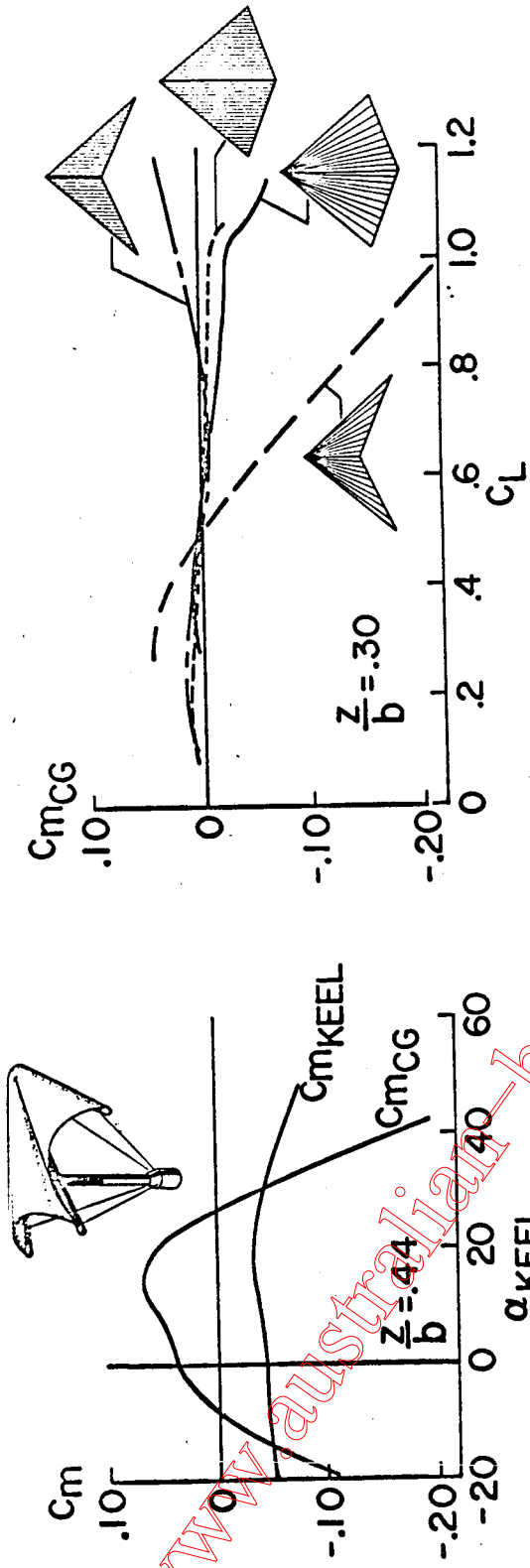


Figure 5.- Pitching-moment characteristics of parawings.

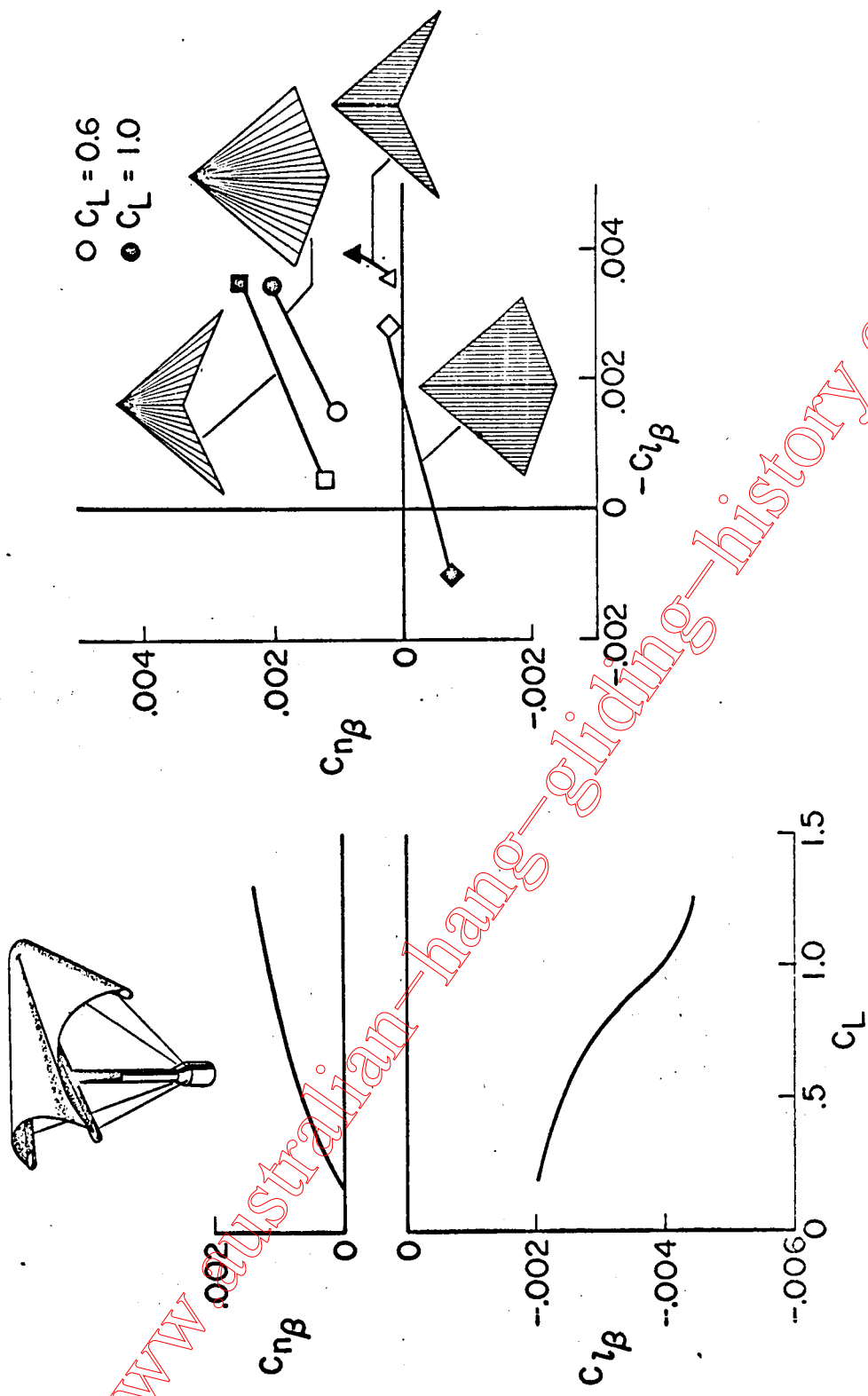
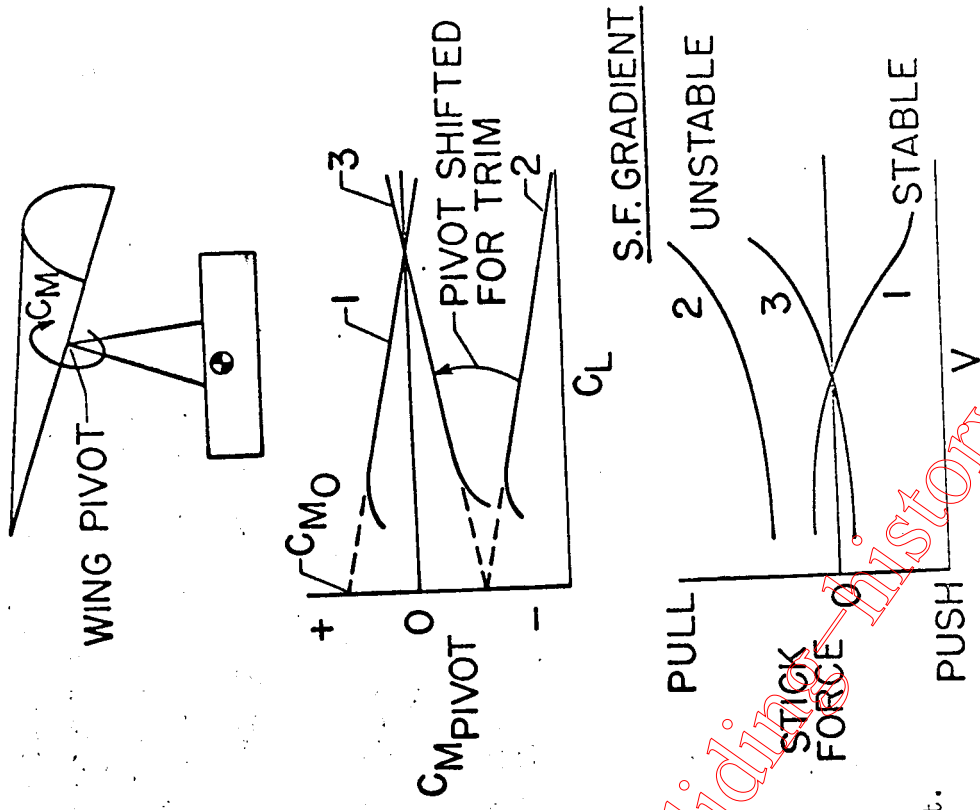
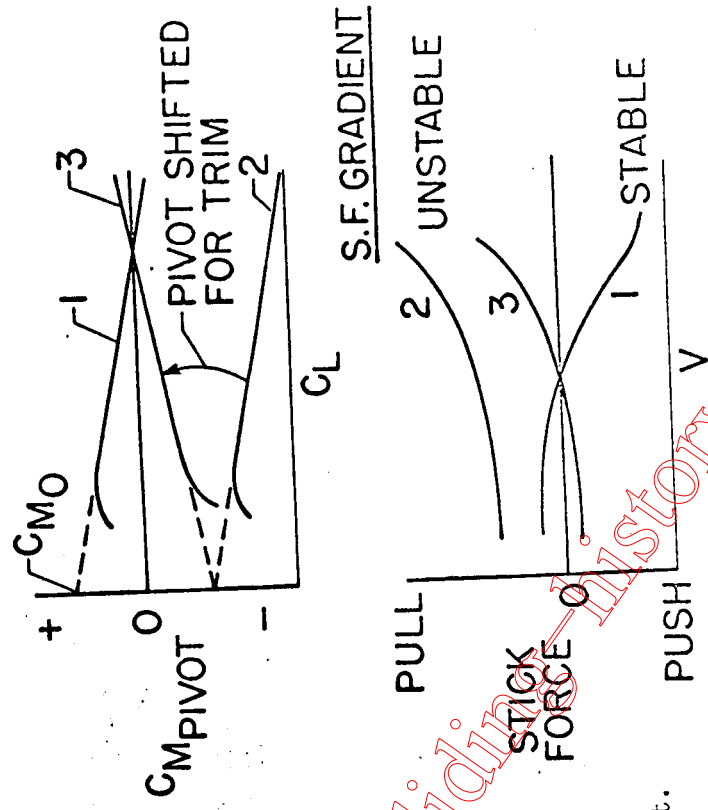
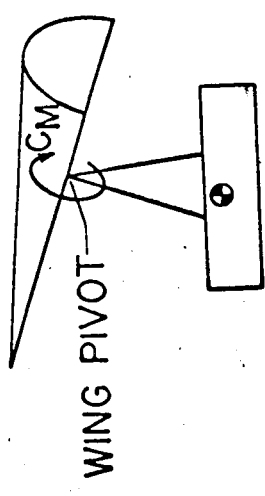


Figure 6.- Static lateral stability characteristics of parawings.



(a) Longitudinal trim by center-of-gravity shift.



(b) Effect of  $C_{m_0}$  on control forces.

Figure 7.- Longitudinal trim and control-force characteristics of parawing configurations.

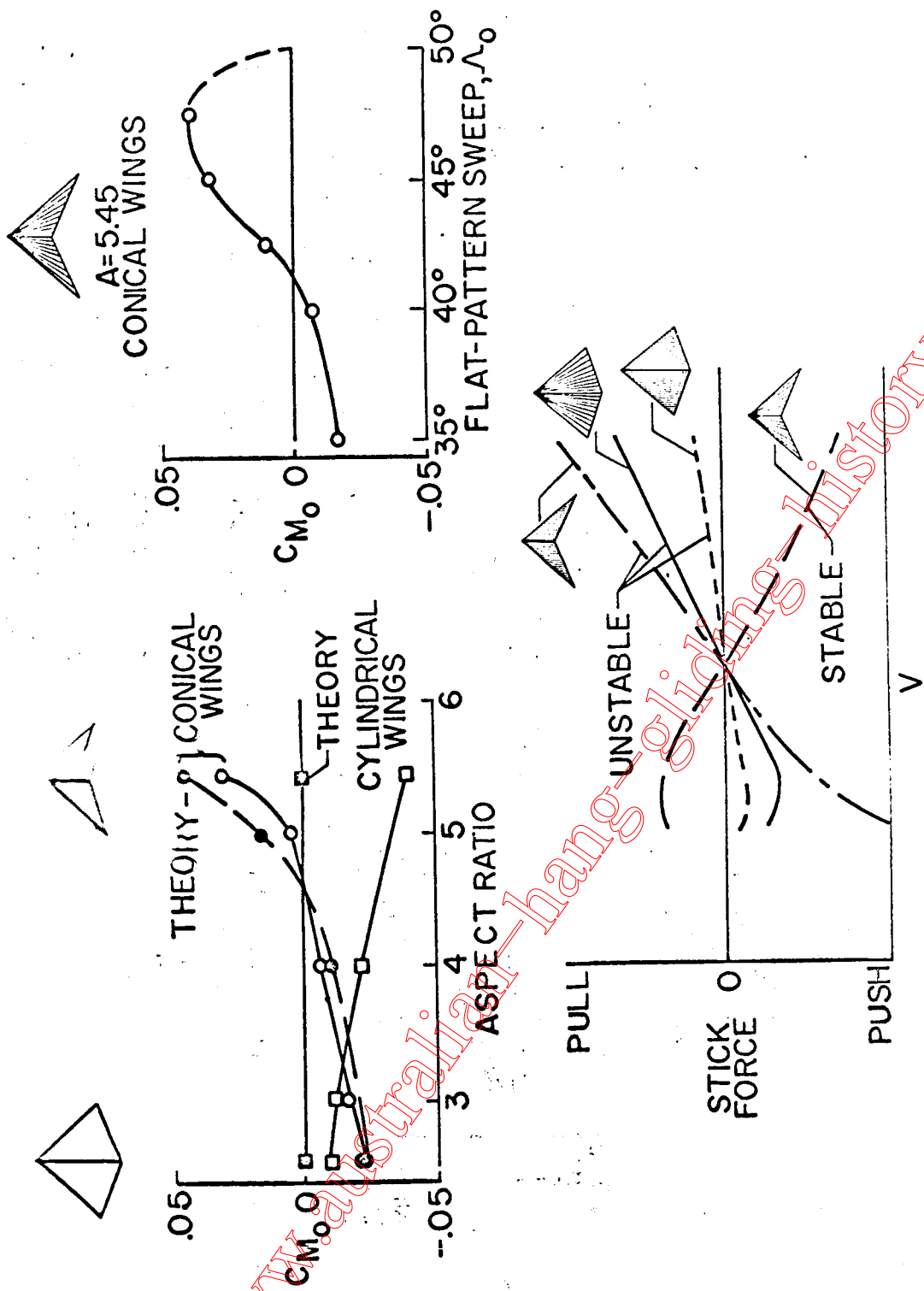


Figure 8.- Effect of wing planform and canopy shape on  $C_{m_0}$  and stick-force gradients.